Metals and Materials International (2018) 24:1309–1314
https://doi.org/10.1007/s12540-018-0136-1

Experimental Verification of the Decomposition of Y_2O_3 in Fe-Based ODS Alloys During Mechanical Alloying Process

Jong Min Byun[1] · Chun Woong Park[2] · Young Do Kim[2,3]

Received: 14 April 2018 / Accepted: 29 April 2018 / Published online: 8 June 2018

Abstract
In this study, we investigated the state of Y_2O_3, as a major additive element in Fe-based ODS alloys, during mechanical alloying (MA) processes by thermodynamic approaches and experimental verification. For this purpose, we introduced Ti_2O_3 that formed different reaction products depending on the state of Y_2O_3 into the Fe-based ODS alloys. In addition, the reaction products of Ti_2O_3, Y, and Y_2O_3 powders were predicted approximately based on their formation enthalpy. The experimental results relating to the formation of Y-based complex oxides revealed that $YTiO_3$ and $Y_2Ti_2O_7$ were formed when Ti_2O_3 reacted with Y; in contrast, only $Y_2Ti_2O_7$ was detected during the reaction between Ti_2O_3 and Y_2O_3. In the alloy of Fe–Cr–Y_2O_3 with Ti_2O_3, $YTiO_3$ (formed by the reaction of Ti_2O_3 with Y) was detected after the MA and heat treatment processes were complete, even though Y_2O_3 was present in the system. Using these results, it was proved that Y_2O_3 decomposed into monoatomic Y and O during the MA process.

Keywords Oxide dispersion strengthened alloy · Y_2O_3 · Mechanical alloying · X-ray diffraction · Thermodynamics

1 Introduction

Fe-based oxide-dispersion-strengthened (ODS) alloys are considered as promising candidates for structural materials in generation-IV reactors, such as sodium-cooled fast reactors and fusion reactors, due to their excellent durability and mechanical properties at high temperatures [1–8]. In Fe-based ODS alloys, oxides, which are very stable even at high temperatures, are used as dispersoids to effectively inhibit dislocation migration. Generally, solid solution strengthening and precipitation hardening, which are the major strengthening mechanisms used for metals, are effective at temperatures up to about 60% of the melting point of the alloy. In contrast, dispersion strengthening is effective at temperatures up to about 90% of the melting point. Therefore, dispersion strengthening by oxide particles is known to be the most effective method for improving the high-temperature mechanical properties and durability of alloys [9–12].

Dispersion strengthening by oxide particles is closely influenced by the size and distribution of the oxide particles [13, 14]. In particular, when the oxide particles are fine and uniformly dispersed, the strengthening effect is stronger [15, 16]. In this context, Y_2O_3 is the most suitable oxide for dispersion strengthening of Fe-based alloys. Y_2O_3 is a very stable oxide in itself but can react with other additive elements during the MA and heat treatment processes, resulting in various types of complex oxides [17–19]. Among the complex oxides that are formed, Y–Ti–O and Y–Hf–O are known to be highly effective for mechanical property enhancement compared to the initial Y_2O_3 [20–24].

However, the formation mechanism of these complex oxides is not yet clear. It is assumed that Y_2O_3 is either amorphized or decomposed and dissolved into the matrix phase during MA; amorphized Y_2O_3 or monoatomic Y reacts with the alloying elements to produce various complex oxides during the heat treatment procedure. Liu et al. [25] carried out MA for up to 48 h with Fe-25 wt% Y_2O_3 powder and reported the amorphization of Y_2O_3 based on the selected area electron diffraction (SAED) patterns of the

✉ Young Do Kim
ydkim1@hanyang.ac.kr

[1] Department of Materials Science and Engineering, Seoul National University of Science and Technology, Seoul 01811, Republic of Korea

[2] Division of Materials Science and Engineering, Hanyang University, Seoul 04763, Republic of Korea

[3] The Research Institute of Industrial Science, Hanyang University, Seoul 04763, Republic of Korea

powder for different milling times. However, several other research groups [26–28] reported the decomposition and dissolution of Y_2O_3 during MA; the X-ray diffraction (XRD) peaks of Y_2O_3 disappeared and the Fe–Cr matrix peaks shifted with an increase in the milling time. The formation mechanism of complex oxides is closely related to their size and dispersion, which are the main variables in determining the properties of Fe-based superalloys. Therefore, the formation mechanism of complex oxides needs to be understood to control and enhance the high-temperature properties of metallic alloys.

This study attempts to verify the formation mechanism of complex oxides through a thermodynamic approach. To this end, Y-based complex oxides that can be produced by the reaction between different elements and Y or Y_2O_3 were investigated based on the reaction enthalpies. The spontaneity of the reaction can be determined by calculating the associated Gibbs free energy change. However, the Gibbs free energies of most Y-based complex oxides are not known. Because the Gibbs free energy is a function of enthalpy, entropy, and temperature, it is understood that enthalpy has a significant effect on the Gibbs free energy in many cases. Therefore, if such a material exists that reacts with both Y and Y_2O_3 and exhibits positive and negative enthalpies in each reaction, it may help in roughly quantifying the reactions of Y and Y_2O_3 and determining the state of matter during the manufacturing process of Fe-based superalloys. It has been confirmed that the reactions of Y and Y_2O_3 with Ti_2O_3 produce different complex oxides; further, such reactions exhibit a significant difference in the reaction enthalpies. In order to verify our assumptions, a Fe–Cr–Ti_2O_3–Y_2O_3 powder was prepared experimentally by an MA process. Alloys were made from this powder by compaction and sintering. The state of Y_2O_3 during the MA process was investigated by analyzing the various oxides formed during the manufacturing process.

2 Experimental Procedures

2.1 Thermodynamic Verification of the Reaction of Ti_2O_3 With Y or Y_2O_3

In this study, 99.9% Y (325 um, RND Korea) and 99.99% Y_2O_3 powders (0.2 um, RND Korea) were mixed with 99.97% Ti_2O_3 powder (43 um, RND Korea) using ball milling and subjected to heat treatment to confirm the thermodynamic data. The raw powders (Nanointech Co., Ltd.) were uniformly mixed using a powder-to-ball weight ratio of 1:15 and a speed of 98 rpm for up to 12 h in an Ar atmosphere. Zirconia balls, 4.8 mm in diameter, were used as the milling media. After the mixing process, the powder mixture was annealed in an Ar atmosphere (99.99% purity, 0.5 L/min flow rate) at 1150 °C for 1 h at a heating rate of 10 °C/min.

2.2 Fe–Cr–Y_2O_3 With Ti_2O_3

99.9% Fe (3–5 μm, Kojundo Chemical Laboratory), 99.97% Cr (43 μm, RND Korea), 99.97% Ti_2O_3 (43 μm, RND Korea), and 99.99% Y_2O_3 (0.2 μm, RND Korea) powders were used as the raw powders. The composition of the samples was set to Fe-20Cr-0.75Ti_2O_3-0.5Y_2O_3. Before the MA process, the internal wall of the grinding jar (SKD 11) was coated using the raw powders with same composition to prevent contamination. The coating was carried out at a speed of 200 rpm for 6 h. Later, the raw powders were weighed and added to the grinding jar for mechanical alloying. The MA process was carried out using a planetary mill (Retsch GmbH, PM400) to crush and uniformly mix the raw powders at a powder-to-ball weight ratio of 1:10 and a speed of 200 rpm for up to 20 h in an Ar atmosphere. Zn stearate (1.4 wt%) was used as the powder control agent and zirconia balls 4.8 mm in diameter were used as the milling media. After the ball milling process, the ball milled-powder was compacted uniaxially by magnetic pulsed compaction (MPC, Nano Technology) at 5 GPa using a cylindrical die of 9 mm diameter. The green bodies were sintered using a tube furnace at 1150 °C for up to 1 h at a heating rate of 10 °C/min in an Ar atmosphere (99.99% purity, 0.5 L/min).

2.3 Analysis

The phases in the ball milled-powders and sintered bodies were investigated using an X-ray diffractometer (XRD; RIGAKU) with Cu Kα radiation of 0.1542 nm wavelength at an operating voltage of 40 kV. The sintered bodies were polished mechanically to 0.1 mm and punched. Subsequently, they were polished electrically at − 10 °C at 15 V and 0.5 A. Methanol (95%, CH_3OH) and 5% perchloric acid ($HClO_4$) were used as the electrolytic solution. The morphologies of the oxide particles were observed using a transmission electron microscope (TEM; Tecnai F20 G2, FEI). Further, the type of oxide was analyzed by selected area electron diffraction (SAED) patterning.

3 Results and Discussion

Table 1 lists the reaction formulae and enthalpies of various complex oxides that can be produced by Y and Y_2O_3 in reaction with Cr, Al, or Ti that are the major additives in Fe-based superalloys. Reaction enthalpy defines the enthalpy change occurring in a system when matter is transformed by a given chemical reaction, when all the reactants and

Table 1 Reaction enthalpies of various complex oxides

Reaction equation	ΔH (kJ/mol)	Reaction equation	ΔH (kJ/mol)
$4Y+2Ti_2O_3+3O_2\rightarrow 4YTiO_3$	−3802	$2Y+2Al+3O_2\rightarrow 2YAlO_3$	−3605
$2Y+Ti_2O_3\rightarrow Y_2Ti_2O_7$	−2400	$2Y_2O_3+4Al+3O_2\rightarrow 4YAlO_3$	−3364
$Y_2O_3+Ti_2O_3\rightarrow 2YTiO_3$	+22	$8Y+4Al+9O_2\rightarrow 2Y_4Al_{12}O_9$	−11,060
$2Y_2O_3+2Ti_2O_3+O_2\rightarrow 2Y_2Ti_2O_7$	−954	$2Y+2Cr+3O_2\rightarrow 2YCrO_3$	−3087
$2Y+2Ti+3O_2\rightarrow 2Y_2Ti_2O_7$	−8001	$2Y_2O_3+4Cr+3O_2\rightarrow 4YCrO_3$	−2328

products are in their standard states. Reaction enthalpy, ΔH_{RXN}, is calculated as follows.

$$\Delta H_{RXN} = \Delta H_P - \Delta H_R.$$

Here, ΔH_P is formation enthalpy of the product and ΔH_R is the formation enthalpy of the reactant.

The spontaneity of a reaction can be determined by calculating the associated Gibbs free energy change. In the case of Y-based complex oxides, there is no lack of information on the Gibbs free energy and the specific heat of the reaction. The Gibbs free energy (G) is a function of enthalpy (H), entropy (S), and temperature (T) ($\Delta G = \Delta H - T\Delta S$). Enthalpy can be calculated by the y-intercept in the formation reaction of the complex oxide. The minimum value of the Gibbs free energy indicates the enthalpy of the reaction because most of the oxide formation reactions proceed towards reducing the overall entropy. Thus, a reaction with lower enthalpy is likely to occur more spontaneously, while a reaction with a positive reaction enthalpy is an involuntary reaction. As shown in Table 1, Cr, Al, and Ti react with Y and Y_2O_3 to produce complex oxides. However, the reactions of Cr, Al, and Ti with Y exhibit lower enthalpies compared to those with Y_2O_3, which is relatively more stable compared to Y. This implies that reactions with monoatomic Y will occur relatively spontaneously. Under such assumptions, $YTiO_3$ can be generated by the reaction of Ti_2O_3 with Y or by the reaction of Ti_2O_3 with Y_2O_3. The enthalpy of the former reaction is –3802 kJ/mol while that of the latter is +22 kJ/mol. Thus, the former reaction may be voluntary while the latter reaction can be involuntary. We can thus conclude by hypothesizing that Ti_2O_3 reacts with Y to produce $YTiO_3$, while the reaction between Ti_2O_3 and Y_2O_3 generates $Y_2Ti_2O_7$, which has a relatively lower reaction enthalpy compared to $YTiO_3$. To verify this assumption, heat treatment was carried out using mixed powders of Ti_2O_3 and Y and Ti_2O_3 and Y_2O_3 at 1150 °C for 1 h.

Figure 1 shows the XRD patterns of the powder mixtures of Y/Ti_2O_3 and Y_2O_3/Ti_2O_3 after heat treatment at 1150 °C for 1 h; on the basis of these results, the type of the complex oxide formed from each reaction could be confirmed. In the XRD pattern of the powder mixture of Y/Ti_2O_3 (Fig. 1a), Y_2O_3, $YTiO_3$, and YTi_2O_6 can be identified. $YTiO_3$ and YTi_2O_6 are intermediate oxides, which are generated due to the lack of Y. Furthermore, XRD peaks

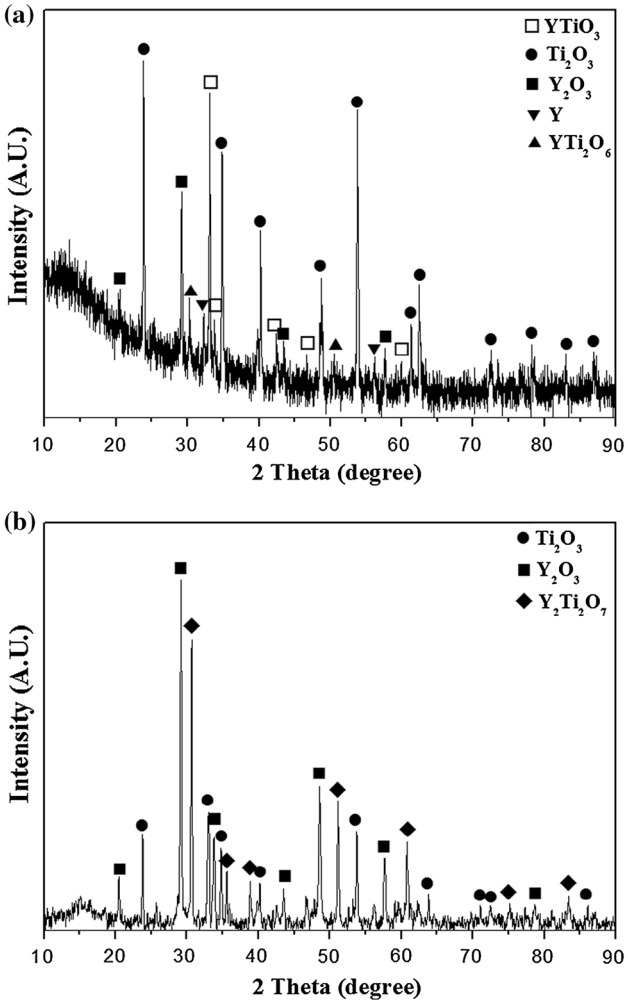

Fig. 1 X-ray diffraction patterns of heat treatment powders. **a** Y/Ti_2O_3 powder mixture and **b** Y_2O_3/Ti_2O_3 powder mixture

corresponding to the raw powders of Y and Ti_2O_3 can be identified. On the contrary, apart from the raw powders of Y and Ti_2O_3, only $Y_2Ti_2O_7$ could be identified from the XRD pattern of the Y_2O_3/Ti_2O_3 mixture (Fig. 1b). Therefore, it was concluded that the state of Y_2O_3 during MA in Fe-based ODS alloys can be identified using Ti_2O_3, which yields different types of complex oxides with Y and Y_2O_3 under the same experimental conditions.

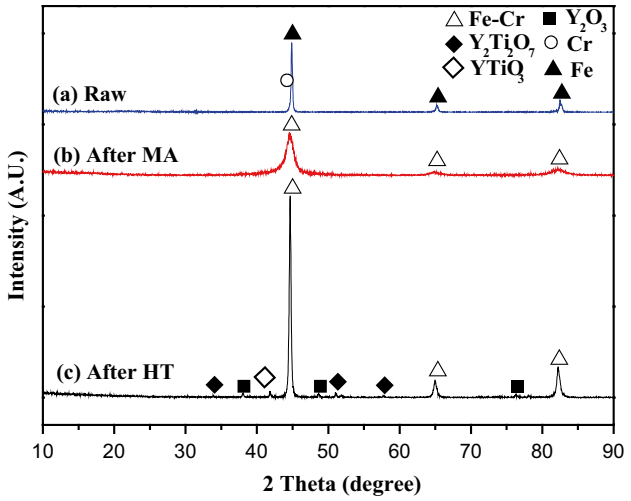

Fig. 2 X-ray diffraction patterns of Fe-20Cr-0.75Ti_2O_3-0.5Y_2O_3 powder; **a** Raw, **b** after MA process, and **c** after heat treatment. (Color figure online)

The XRD pattern of an Fe-20Cr-0.75Ti_2O_3-0.5Y_2O_3 powder after MA for 20 h and an Fe-20Cr-0.75Ti_2O_3-0.5Y_2O_3 powder compacted and heat treated at 1150 °C for 2 h are shown in Fig. 2. First of all, in the mixture of the raw powders, only the peaks corresponding to Fe and Cr raw materials could be identified but the peaks corresponding to Ti_2O_3 and Y_2O_3 could not be identified due to their relatively small proportions in the mixture. In the case of the Fe-20Cr-0.75Ti_2O_3-0.5Y_2O_3 powder subjected to MA process, only a Fe–Cr peak, which indicates that Cr atoms enter into solid solution in Fe, could be identified. Peaks of Ti_2O_3 and Y_2O_3 were not present in the X-ray diffraction patterns. However, in the case of the heat-treated Fe-20Cr-0.75Ti_2O_3-0.5Y_2O_3 powder, peaks of Y_2O_3, $Y_2Ti_2O_7$, and $YTiO_3$ were identified in addition to the peaks corresponding to Fe–Cr. Of these complex oxides, $YTiO_3$ is produced by the reaction of Y with Ti_2O_3 as confirmed experimentally by the reaction of Ti_2O_3 with Y or Y_2O_3 powder. Therefore, it is determined that the added Y_2O_3 exists as monoatomic Y within the matrix phase because it is resolved during the MA process.

Elemental mapping of Fe-20Cr-0.75Ti_2O_3-0.5Y_2O_3 sintered sample was analyzed using energy dispersive X-ray spectroscopy with scanning transmission electron microscopy (STEM). As shown in the high angle annular dark field (HAADF) image in Fig. 3, nanosized oxide particles with different sizes are uniformly distributed within the matrix phase. In addition, EDS mapping analysis was carried out

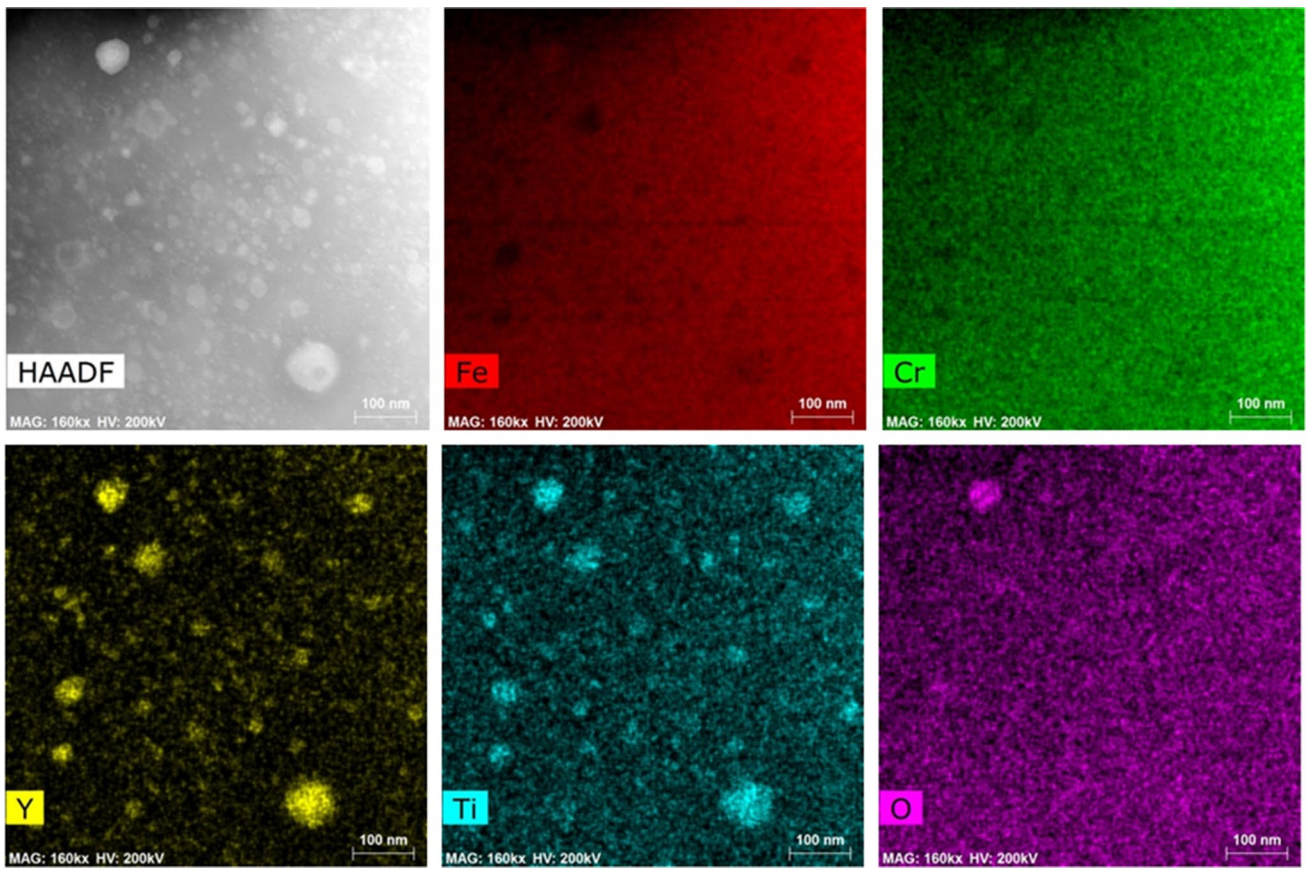

Fig. 3 STEM-EDS images of Fe-20Cr-0.75Ti_2O_3-0.5Y_2O_3 sintered specimens. (Color figure online)

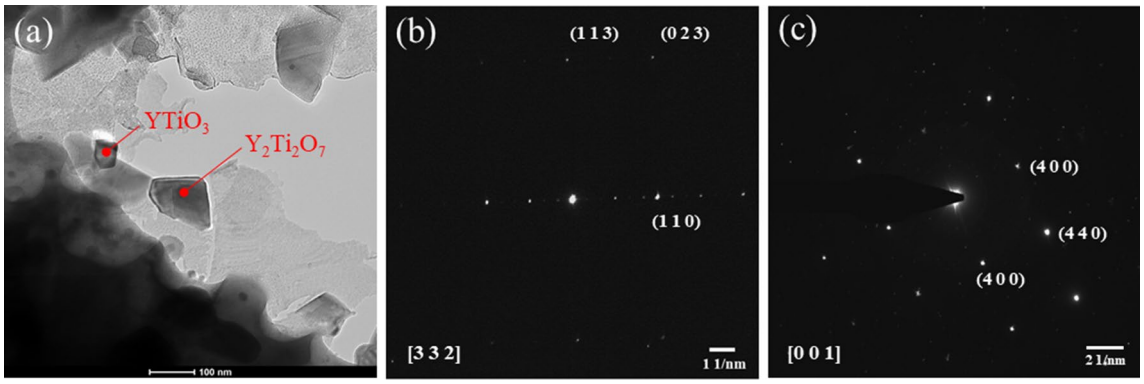

Fig. 4 TEM image and SAED patterns. **a** TEM image of complex oxides, **b** $YTiO_3$ SAED patterns, and **c** $Y_2Ti_2O_7$ SAED patterns. (Color figure online)

to analyze the composition of oxides. The distribution of Fe and Cr and that of Y, Ti, and O matched each other exactly. Thus, it is believed that nanosized Y–Ti–O oxides are uniformly distributed within the matrix phase of Fe–Cr.

The structural analysis with TEM of the oxides in Fe-20Cr-0.75Ti_2O_3-0.5Y_2O_3 sintered sample are shown in Fig. 4. $YTiO_3$ (Fig. 4b) and $Y_2Ti_2O_7$ (Fig. 4c) of SAED patterns were indexed to an orthorhombic [322] zone orientation with lattice parameters (a: 5.6890 A, b: 7.6094 A, c: 5.3350 A) and a cubic [001] zone orientation with lattice parameter (a: 10.09 A), respectively. Furthermore, these results agreed well with the results of the XRD analysis. The existence of $YTiO_3$ also confirms the existence of monoatomic Y during the manufacturing process.

4 Conclusions

Heat treatment of a mixed powder comprising Y, Y_2O_3, and Ti_2O_3 resulted in the formation of Y-mixed Ti_2O_3 powder, Y_2O_3, $YTiO_3$, and YTi_2O_6, as well as raw powders of Y and Ti_2O_3, which were identified. Y, Ti_2O_3, and $Y_2Ti_2O_7$ could be identified in the case of the Y-mixed Ti_2O_3 powder. Further, in the sample subjected to MA process and heat treatment at 1150 °C for 20 h, complex oxides of $YTiO_3$ that can only be formed by the reaction of Ti_2O_3 with monoatomic Y were identified.

Acknowledgements This research was supported by the Technology Innovation Program (10048158, Development of 980 °C grade superalloys strengthened by multi-component nano-oxides for commercialization of core materials in the field of the defense industry) funded by the Ministry of Trade, Industry and Energy (MI, Korea). This research was also supported by the Basic Science Research Program through the National Research Foundation of Korea (NRF) funded by the Ministry of Education of Korea (2016R1A6A1A03013422).

References

1. A. Kimura, R. Kasada, A. Kohyama, H. Tanigawa, T. Hirose, K. Shiba, S. Jitsukawa, S. Ohtsuka, S. Ukai, M.A. Sokolov, R.L. Klueh, J. Nucl. Mater. **367–370**, Part A (2007)
2. R.L. Klueh, J.P. Shingledecker, R.W. Swindeman, D.T. Hoelzer, J. Nucl. Mater. **341**, (2005)
3. M.L. Flem, in *Advanced Materials for Fuel Cladding in Sodium Fast Reactors*, Presentation to 3rd MATGEN Summer School, Lerici, Italy, 2011
4. P. Norajitra, R. Giniyatulin, T. Ihli, G. Janeschitz, P. Karditsas, W. Krauss, R. Kruessmann, V. Kuznetsov, D. Maisonnier, I. Mazul, C. Nardi, I. Ovchinnikov, S. Papastergiou, A. Pizzuto, P. Sardain, Nucl. Fusion **45**, 11 (2005)
5. T.R. Allen, J. Gan, J.I. Cole, M.K. Miller, J.T. Busby, S. Shutthanandan, S. Thevuthasan, J. Nucl. Mater. **375**, 1 (2008)
6. J.H. Lee, J.H. Kim, J. Kor. Powder Met. Inst. **20**, 3 (2013)
7. S. Ukai, T. Okuda, M. Fujiwara, T. Kobayashi, S. Mizuta, H. Nakashima, J. Nucl. Sci. Technol. **39**, 8 (2002)
8. M. A. Sokolov, H. Tanigawa, G. R. Odette, K. Shiba, R. L. Klueh, J. Nucl. Mater., **367–370**, Part A (2007)
9. A. Kelly, R.B. Nicholson, *Strengthening Methods in Crystals* (Wiley, New York, 1972)
10. M.J. Alinger, Dissertation, University of California, Santa Barbara, 2004
11. Z. Oksiuta, M. Lewandowska, K.J. Kurzydolwski, Mech. Mater., **67**, (2013)
12. H. Xu, Z. Lu, S. Ukai, N. Oono, C. Liu, J. Alloys Compd., **693**, (2017)
13. G.J. Zhang, Y.J. Sun, R.M. Niu, J. Sun, J.F. Wei, B.H. Zhao, L.X. Yang, Adv. Eng. Mater. **6**, 12 (2004)
14. M. A. Auger, T. Leguey, A. Munoz, M. A. Monge, V. D. Castro, P. Fernandez, G. Garces, R. Pareja, J. Nucl. Mater., **417**, (2011)
15. I.S. Kim, B.Y. Choi, C.Y. Kang, T. Okuda, P.J. Maziasz, K. Miyahara, ISIJ Int. **43**, (2003)
16. M. A. Auger, V. D. Castro, T. Leguey, A. Munoz, R. Pareja, J. Nucle. Mater., **436**, (2013)
17. H. Sakasegawa, M. Tamura, S. Ohtsuka, S. Ukai, H. Tanigawa, A. Kohyama, M. Fujiwara, J. Alloys Compd., **452**, (2008)
18. P. Unifantowicz, T. Plocinski, C. A. Williams, R. Schaublin, N. Blanc, J. Nucl. Mater., **442**, (2013)
19. K. Oka, S. Ohnuki, S. Yamashita, N. Akasaka, S. Ohtsuka, H. Tagigawa, Mater. Trans., **48**, (2007)
20. Q. Tang, T. Hoshino, S. Ukai, B. Leng, S. Hayashi, Y. Wang, Mater. Trans. **51**, 11 (2010)

21. H. Sakasegawa, S. Ohtsuka, S. Ukai, H. Tanigawa, M. Fujiwara, H. Ogiwara, A. Kohyama, J.Nucl. Mater., **367-370**, Part A (2007)
22. M. A. Moghadasi, M. N-Ahmadabadi, F. Forghani, H. S. Kim, Sci. Rep., **6**, (2016)
23. M. J. Alinger, G. R. Odette, D. T. Hoelzer, Acta Mater., **57**, (2009)
24. D.J. Larson, P.J. Maziasz, I.-S. Kim, K. Miyahara, Scr. Mater. **44**, 2 (2001)
25. T. Liu, H. Shen, C. Wang, W. Chou, Prog. Nat. Sci. **23**, (2013)
26. Y. Kimura, S. Takaki, S. Suejima, R. Uemori, H. Tamehiro, ISIJ Int. **39**, (1999)
27. L. Barnard, N. Cunningham, G.R. Odette, I. Szlufarska, D. Morgan, Acta Mater. **91**, (2015)
28. P. He, T. Liu, A. Möslang, R. Lindau, R. Ziegler, J. Hoffmann, P. Kurinskiy, L. Commin, P. Vladimirov, S. Nikitenko, M. Silveir, Mater. Chem. Phys. **136**, (2012)